

Consequences of covid-19: urban thermal variation and social repercussion

ABSTRACT

Thermal variation is a common urban phenomenon, from small to large cities, both due to anthropic origin and natural causes. Due to the influence of COVID 19, there was a reduction in social activities, mainly economic, which impacted both industrial production and the decrease in vehicle circulation. Such changes in habits affect urban thermal dynamics. Thus, the objective of the study is to identify whether the reduction of socioeconomic activities has affected the patterns of thermal variation in Curitiba, Brazil. For this analysis, Landsat 8 images from the years 2018, 2019 and 2020 were used to verify the temperature variation in the region, and the NDVI index was applied to verify the variation in permeable area in the capital. Thus, it was possible to observe that the average total surface temperature of Curitiba decreased by 1.6° C. It was also seen that in some areas the reduction was greater than others, and the variation between minimum and maximum temperature was 13.3° C. It is noteworthy that due to the reduction in green areas in the region, an increase in temperature was expected. The areas with the greatest change in temperature in degrees were those with large roads in Curitiba, places whose population has a low salary compared to more central neighbourhoods in the city. Although the virus raises great concern about the health of the population, a significant decrease in temperature can be observed, mainly caused by the circulation of vehicles.

KEYWORDS: Urban Heat Island, Environmental health, Landsat 8

Mayara Bormann Azzulin

mayarabormann@gmail.com

Universidade Tecnológica Federal do Paraná. Curitiba. Paraná. Brasil.

Adrian Jedy

adrianjedyn@gmail.com

Pontifícia Universidade Católica do Paraná. Curitiba. Paraná. Brasil.

Nicole Centurion

centurion.nicole@gmail.com

Pontifícia Universidade Católica do Paraná. Curitiba. Paraná. Brasil.

Valdir Fernandes

vfernandes@utfpr.edu.br

Universidade Tecnológica Federal do Paraná. Curitiba. Paraná. Brasil.

1 INTRODUCTION

As the rapid urbanization occurs, changes of land use and land cover (LULC) are observed, which consequently cause numerous unwanted environmental impacts (Sánchez-Reyes et al., 2017; Golden, 2004). Due to human activities, the crescent demographic growth in urban areas leads to changes in natural cycles.

Over time, this can be translated to significant increases in micro and mesoscale temperatures compared to rural areas in the same region (Golden, 2004). Changes in land cover pattern interferes with the temperature on a local scale (Rahaman et al., 2018), as the characteristics of each surface affects energetic flows and balance, which ultimately results in alterations in the urban climate (Ferreira & Andrade, 2021).

This happens because of factors such as mobility, consisting in the locomotion of people among spaces, and the radiation emitted or reflected by the diverse materials and surfaces that compose urban landscapes (Neves et al., 2018).

Urban heat islands (UHI) are characterized by the simultaneous difference in air and soil temperature between urban areas and their rural surroundings (Ding & Shi, 2013). Its intensity varies according to environmental factors, such as local and synoptic climate, season, time of day, size, and geographic location of the city (Essa et al., 2013). Also, anthropogenic heat originated from activities such as factory production, transportation and the heat released from homes (Weng & Yang, 2006), contribute to that phenomenon.

Monitoring this phenomenon allows development of strategies to mitigate its negative effects. However, the analysis of the incidence of UHI is hampered by the complexity of factors involved in its assessment and conceptualization (Ferreira & Andrade, 2021). Therefore, a localized approach to the effects is essential to understand its implications.

Also, natural factors such as El Niño and La Niña affect cities' temperature. According to the report by the United States National Oceanic and Atmospheric Administration Service (NOAA) published on February 14, 2019, the El Niño period in Brazil reached its peak in the period between the months of January and March. This atmospheric-oceanic phenomenon is characterized by a temperature increase of Tropical Pacific Ocean's waters, directly affecting the regional and global climate (NOAA, 2020).

Curitiba has extensive vegetation cover and a historical concern with urban management and planning, and even so, it presents points of attention regarding its microclimate. Ferreira & Andrade (2021) identified in their study the presence of daytime heat islands of + 1.5°C in relation to their surroundings, and in the night period of 3 to 4.4°C, the greatest intensity among Brazilian metropolises, between 2000 and 2016. The highest intensity of UHI was observed in the hottest seasons, and despite the similar average UHI intensity in the winter, the maximum intensity is significantly lower (Krüger, 2015).

UHI is related to the incidence of locations of heightened disease risk, such as dengue fever. Lunardon (2017) pointed out that there are greater risks regarding the proliferation of the disease vector in Curitiba neighborhoods with a higher incidence of the heat island effect.

In view of the incidence of coronavirus in Brazil, one of the measures to prevent infection and spread of the disease in the Brazilian population is social isolation. This measure directly influences the habits of the population, with the main highlight being the circulation of vehicles and lessened industrial activities, which supposedly brings a reduction in the average temperature of the earth's surface.

The impact on global temperature due to the short-term effects of the pandemic is likely to be of low magnitude (Forster et al., 2020), mainly due to the time scale in which the event occurs. Effective global climate change is only considered when there are noticeable statistical differences between two climatological normals (Chung, Choi & Yun, 2004), although, these alterations can be consolidated in the long term if significant changes in urban lifestyles occur.

Thus, this work will identify how the diminished urban activities, such as vehicle mobility, has affected the thermal variation regimes in the Brazilian city of Curitiba, and where these variations occur. The results made it possible to identify the influences of pandemic mitigation measures on urban.

2 THEORETICAL FOUNDATIONS

2.1 Covid-19

Coronavirus disease 19 (COVID-2019) is an infectious disease identified in Wuhan, Hubei province, China in December 2019. On February 25, 2020, 2700 deaths were counted (Wang et al., 2020) and 12 April reached 106,138 fatalities (WHO, 2020).

There are numerous precautions recommended to contain the spread of contagion of respiratory tract diseases, such as increasing ventilation in closed environments, using masks, washing hands and social isolation (Zhang et al., 2018). In response to the spread of the disease, several countries have adopted containment and mitigation initiatives to reduce hospitalization peaks and avoid excessive demand for hospital beds, this added to the protection of populations most vulnerable to infection (Bedford et al., 2020), which it can be decisive in preventing the collapse of national health systems.

In the case of COVID-19, seen that it is still a recent and poorly understood phenomenon, there are many uncertainties. As new research emerges, it is identified that the virulence of the disease allows transmissions from one to two days after infection, similar to the behavior of influenza A and distinctly from SARS. In SARS, the peak of infectivity occurs several days after the first symptoms, which justifies the successful quarantine of infected patients and the lack of success of this measure for influenza A, and possibly for COVID-19 (Anderson et al., 2020).

Disease transmission vulnerability is more pronounced in urban areas, due to population concentration, increasing the probability of transmittal of pathogens and the maintenance of infection chains (Keil & Ali, 2007). Work interruptions and school closures have been shown to be effective in protecting the population from the incidence of infectious respiratory diseases. The permanence of infected people in their homes has a direct impact on community transmission, but the

effectiveness of this approach is low if no other containment measures are taken (Zhang et al., 2018).

Owing to contagion risk, Wuhan's unofficial access and exit transit was closed in January, and then isolation and quarantine policies were implemented nationally (Wang et al., 2020). Epidemics of infectious diseases cannot be contained with local public health strategies, requiring multi-scale approaches, such as isolation and quarantine (Keil & Ali, 2007).

The reduction in productive activities and restrictions on outdoor activities in China, caused a contraction in the pollutants emission pollutants from transport and industry in several cities and provinces, during this period. However, severe pollution events were not impacted (Wang et al., 2020). Similarly, the SARS crisis has changed the balance of social, economic, and environmental interests in the elite and popular circles that constitute the governments of the affected places (Keil & Ali, 2007).

2.2 Urban heat

Cities are constituted by densely inhabited landscapes in which the human presence is connected to biophysical properties. They are characterized by small-scale mosaics with diverse types of land use, most of which have structures originating from nature and the human environment (Andersson, 2018).

They are associated with several negative environmental factors, such as pollution, ozone depletion and greenhouse gas emissions (Weng & Yang, 2006). This is a result of anthropogenic changes in LULC patterns, having a direct and permanent influence on the ecosystem. Therefore, cities are ecological systems distinct from rural surroundings, with significant differences in soils, hydrology, and climate (Kowarik, 2011).

Quantifying urban environmental quality is an intricate activity, as it derives from natural factors that vary in wide space-time scales, as well as local factors in the infrastructure originated by human activity (Nichol & Wong, 2005), such as buildings and roads.

As an evidence of this, urbanization causes disturbances in the terrestrial energy balance, because of the removal of vegetation and impermeabilization of the surface, presenting greater absorption of solar radiation and greater thermal capacity and conductivity. In addition to this, urban dynamics and anthropic activities give rise to urban heat islands (Weng & Yang, 2006), resulting in a thermal scenario comparable to what is expected from the implications of the greenhouse effect (Xian & Crane, 2006).

Ding and Shi (2013) identified an evident temperature gradient between rural and urban areas, with higher temperatures closer to the city centre, because the urbanized surface, composed of streets and buildings made of asphalt and concrete, has a higher radiant temperature. Each component of surfaces in cities has different radiant, thermal, moisture and aerodynamic properties, and this has implications for their surrounding environment (Weng & Yang, 2006).

The study by Rahaman et al. (2017), demonstrated that in the more urbanized areas of Alberta (Calgary, Edmonton and Fort McMurray), local temperature increased significantly, possibly due to uneven changes in land use. The authors

also warn of possible impacts to the biota of the places affected by local climate change, which must be considered by public managers.

Thermal variation within urbanized areas also results from spatial occupation parameters such as the morphological characteristics of the built environment (Essa et al., 2013), seen that temperatures are lower in places with low temperature density and relationship between pavement and area. Other factors that cause spatial effects of thermal imbalance are income, level of education and ethnic and racial characteristics that affect population location and housing conditions (Yin et al., 2018).

These changes in urban surfaces affect the thermal variation on a fine spatial scale (Rahaman et al., 2018), therefore, making it difficult to map by the conventional method, using climatological stations. One of the problems that can be accentuated by this difficulty of monitoring, refers to the vulnerability of certain social groups to extreme heat fluctuations, as is the case of people over the age of 65 years. The determination of strategies to mitigate these localized phenomena depends on spatialized information with high resolution, so that effective planning can be done (Lapola et al., 2019).

It is extremely important to obtain empirical evidence for predicting temperature changes at the local scale, especially regarding situations susceptible to natural disasters and the management of natural resources (Rahaman et al., 2018).

2.3 Urban heat and mobility

The transition from natural soil cover to built environment generates numerous impacts, such as the modification of the initial climate conditions. One of the most affected aspects of the city-atmosphere system, corresponds to the urban thermal field (Barbosa, 2009). Terrestrial energy balance is impaired and destabilized, due to the large amounts of energy stored in the urban surfaces throughout the day and that are subsequently released at dusk (Golden, 2004).

Therefore, there is an increase in temperatures, which are aggravated by other anthropic sources such as the use of air conditioners, machines, and motor vehicles (Golden, 2004; Haddad & Aouachria, 2015).

Motor vehicles emit total heat, which remains confined to urban spaces without ventilation, impairing the thermal comfort of the environments (Haddad & Aouachria, 2015). In addition, the consumption of fossil fuel, the emission of carbon dioxide and other greenhouse gases, which contribute to the intensification of urban heat islands as well as global warming (Kolbe, 2019).

When considering urban environments and opportunities for work, education, health, and housing (Haddad & Aouachria, 2015; Yamak et al., 2021), the need for the development of mobility mechanisms is increasing, especially in view of its purpose of facilitating “the displacement of people and goods in the city due to its complex activities” (Araujo et al., 2011).

In the study by Palme et al. (2016), developed in South American cities, significant changes (between 20 to 59%) were detected in the resulting urban heat islands due to the increase in traffic. The morphological density of the cities in

question was also identified as an important factor for the phenomenon, in some cases increasing its intensity, or decreasing it (Palme et al., 2016).

Forster et al., (2020), while analyzing the period of March and April of 2020 - in which measures of social distancing were implemented in most countries - found in their study a reduction of pollutants CO₂ and NO_x by approximately 30% in April, due to the decline in emissions by surface vehicles, while organic carbon increased due to increased residential emissions.

However, transport systems' development and the multiplication of individual modes, has contributed to traffic congestion, the increase in travel times, loss of mobility of people, wasted energy, accidents, and increased pollution (Boareto, 2008). Such is the extent of its impact on the environment, that mobility itself is a major problem for sustainable development (Kolbe, 2019). Environmental issues and atmospheric pollution cause many social problems, since despite the widespread reach of the pollution, its impacts are more prominent in the health of socially vulnerable, such as the poverty-stricken, in reason of greater exposure to disease and the lack of resources for treatment (Boareto, 2008).

3 MATERIALS AND METHODS

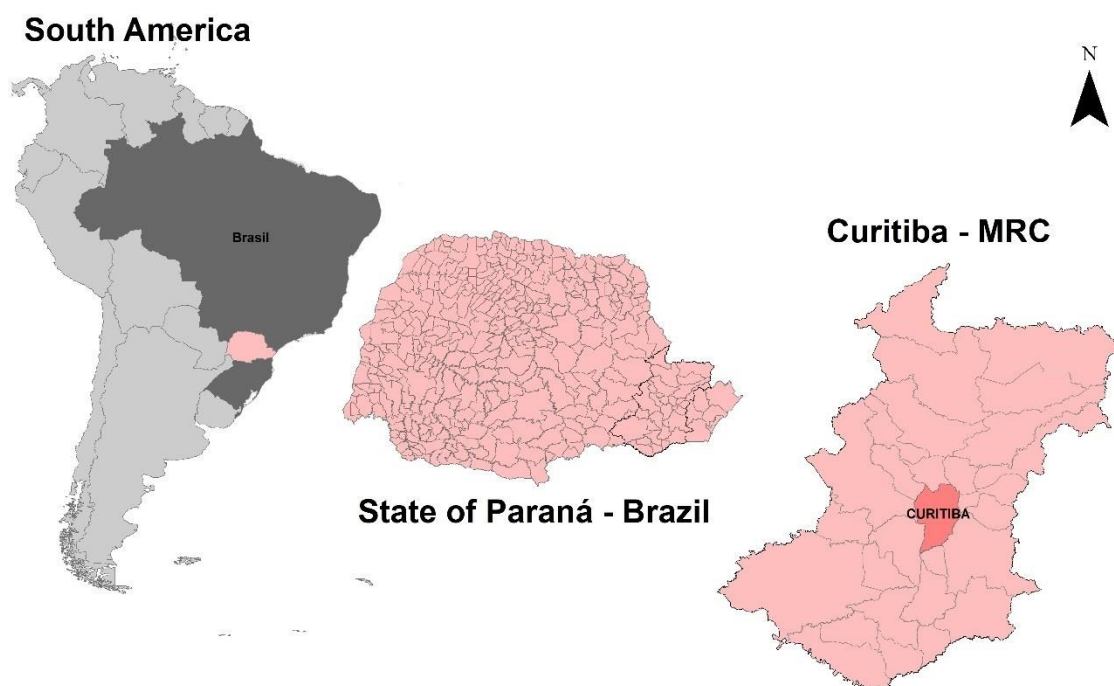
Geoprocessing was used to ascertain the variation in surface temperature of the studied area during the month of March in the years 2020, 2019 and 2018, as well as to identify the points of the city with the most significant thermal variation.

Finally, images and data were collected from the Google Maps application (GOOGLE, 2020), for qualitative and descriptive visual assessment of the observed thermal variation points.

3.1 Study area

The area to be studied is the city of Curitiba, which is the capital of the state of Paraná in Brazil (Figure 1). The city has 1,993,105 inhabitants (IBGE, 2020), and the population of the Metropolitan Region of Curitiba (MRC) is 3,615,027 inhabitants (IBGE, 2020).

Figure 1 - Study area



Source: the authors, 2020.

The climate in Curitiba is oceanic (cfb), with a summer that is more humid than winter and the rains distributed throughout all seasons of the year. Average temperatures fluctuate in the summer between 17 to 20°C and in the winter between 12-14°C, while the annual average is 16°C. The thermal range varies from 0.5°C to 25.7°C, with an average of 10.5°C. For the month of March, the average temperature in the climatological normal is 20.1°C for the period from 1981 to 2010 (INMET, 2020).

According to Research of Origin and Destination (2017), carried out by the Institute of Research and Urban Planning of Curitiba, there are many motor vehicles that circulate in the region, both for collective and individual transport. According to the same survey, the main reason for trips between Curitiba between the metropolitan region is housing (close to 50%), followed by work (average 20%) (IPPUC, 2013).

3.2 Data characteristics and specifications

Due to the nature of the research, several sets of data were acquired to perform the thermal analysis in the chosen territorial and temporal coverage.

The analysis is limited within the perimeter of the city of Curitiba, using as a base the vector file provided by the Institute of Research and Urban Planning of Curitiba - IPPUC, with UTM projection, Datum Sirgas 2000 and spindle 22 South (IPPUC, 2020), which were ultimately converted to the WGS84 standard, for further analysis.

Multispectral images were selected from the LANDSAT 8 OLI-TIRS satellite for the month of March of the years 2018, 2019 and 2020. March is of important

significance to this study, since is the month that social distancing initiatives started in Curitiba. A reduced time span was used to minimize distortions caused by the urbanization process itself - that is, changes in land use (LULC) - and global climate changes that occur over the long term.

Scenes with similar weather conditions were selected in the same chronological period (Table 1)

Table 1 - Landsat 8 scenes used

File Date	Satellite/ Sensor	Path	Row	Cloud cover (%)	Hour (GMT)
2020-03-19	Landsat 8 OLI-TIRS	220	078	3.84	20:52
2019-04-21	Landsat 8 OLI-TIRS	220	078	2.92	20:14
2018-03-20	Landsat 8 OLI-TIRS	220	078	53.20	16:10

Source: USGS (2020).

Although the percentage of cloud cover is greater than 50% in the 2018 image, they do not reach the studied area, therefore not affecting the study.

The OLI sensor uses nine spectral bands in the visible and infrared range of short wave, complemented by two thermal channels. Unlike the other satellites of the Landsat mission, the addition of band number 1 (Aerosol) stands out, planned for better detection of chlorophyll and other materials suspended in coastal waters, and 9 with greater cloud detection capacity (Table 2).

Its radiance quantization is in 12 bits, which can iterate 4096 different values, which improves the measurement of the variability of surface conditions, unlike the 4-7 series Landsat satellites, which quantify their data in 8 bits, which can have 256 different values (Roy et al., 2014).

Table 2 - Landsat 8 OLI-TIRS specifications

Color	Wavelength (µm) - Band	Resolution (m)
Costal/ aerosol	0,43-0,45 – Band 1	30
Blue	0,45-0,51 – Band 2	30
Green	0,53-0,59 – Band 3	30
Red	0,64-0,67 – Band 4	30
NIR	0,85-0,88 – Band 5	30
SWIR 1	1,57-1,65 – Band 6	30
SWIR 2	2,11-2,29 – Band 7	30
Pancromatic	0,50-0,68 – Band 8	15
Cirrus	1,36-1,38 – Banda 9	30
TIRS 1	10,60-11,19 – Banda 10	30(100*)
TIRS 2	11,50-12,51 – Banda 11	30(100*)

Source: Adapted from Roy et al. (2014), Estoque et al. (2017) and Young et al. (2017).

* TIRS bands are acquired at the resolution of 100m, but resampled to 30m in the final product (Estoque et al., 2017).

Landsat 8 has orbital characteristics that allow revisiting within 16 days (Roy et al., 2014). It is a long-time window in studies related to temperature, especially when compared to sensors such as MODIS (Moderate Resolution Imaging Spectroradiometer) with temporal resolution of one day. The LANDSAT 8 satellite was used due to its spatial resolution of 30m (each pixel represents a 900m² grid), while in the MODIS sensor the resolution varies from 250m to 1000m depending on the band used (Rahaman et al., 2018), considerably more coarse, inadequate for the scale of the study.

To perform the temperature analysis, images from the LANDSAT-8 satellite were used, corresponding to the 10.4–12.5 µm wavelength (band 10), obtained by the Thermal Infrared Sensor (TIRS). For the vegetation index, it was used the band 4 (red color - 0.630 to 0.680 µm) and the band 5 (near infrared - 0.845 to 0.885 µm).

For the treatment of the raster data, the Curitiba area was selected, and the scenes were intersected with the city limits vector, followed using the fixed data of conversion of grey levels of the image (NC) to radiance at the top of the atmosphere (TOA radiance), using the equation (eq. 1):

$$L\lambda = MI * Qcal + AL$$

(1)

$L\lambda$ corresponds to TOA Radiance (Spectral Radiance of the Aperture Sensor in Watts), MI is the multiplicative factor of scaling of band 10 available in the metadata of the satellite image, Qcal refers to the digital number (DN) which is the

value of pixel of the band, and finally, AL which is the specific additive scaling factor of the band (USGS, 2020).

The data set obtained was validated by means of a comparative analysis between the data extracted by processing satellite images and the historical data of climatic stations made available by the platform of the Meteorological Database for Teaching and Research (BDMEP) of the National Institute of Meteorology (INMET). In the city of Curitiba there are two such stations (Table 3), one automatic (A807) and the other conventional (83842) (INMET, 2021).

Name	Operation	Latitude	Longitude	Altitude(m)
83842	Conventional	-25.4486	-49.2305	923.5
A807	Automatic	-25.4486	-49.2305	922.9

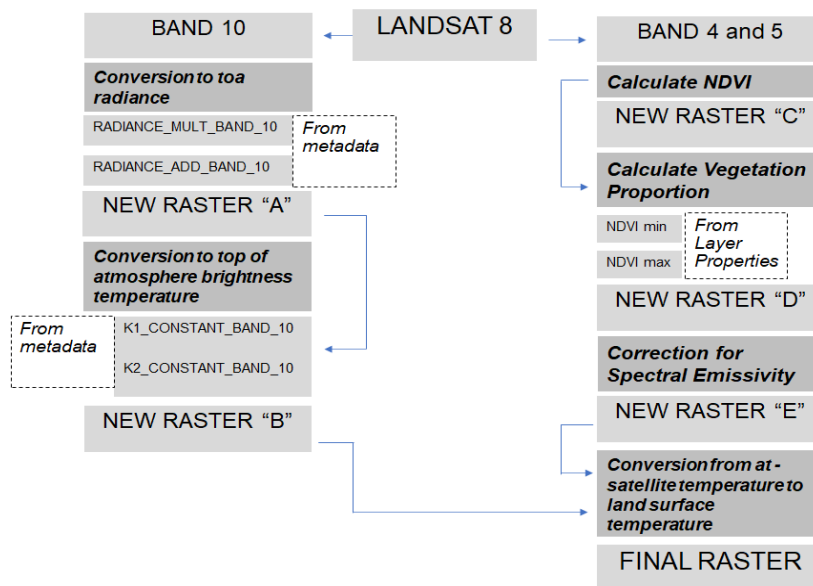
Source: INMET (2020).

3.3 Calculating the surface temperature in the study area

Surface temperature is an important variable for urban climatology, used to estimate liquid irradiation, sensible and latent heat flow, thermal inertia, intensity of heat island, perceived water, evapotranspiration, surface runoff and surface moisture (Essa et al., 2013).

Local heating trends are commonly calculated with historical temperature data in climatological stations, but in situations where there are limitations to their use, interpolation methods based on geographic information systems (GIS) are used (Rahaman et al., 2017). Specifically, to the territorial coverage studied, with a scarcity of spatial thermal data due the shortage of stations, geoprocessing is an essential tool to understand the urban climate, but make use of this tool, it is necessary to process the data in different ways to carry out the intended analyses (Figure 2).

Figure 2 - Satellite data processing schematics



Source: The Authors, 2020.

GIS technology allows the cross evaluation of data from different sources and the analysis of numerous spatial variables, such as urban land use, pollution, and thermal variation in an urban context (Weng & Yang, 2006).

Comparing research methods that use data obtained from surveys of meteorological stations, remote sensing provides information with greater spatial resolution on changes in soil cover and temperature variation, however, being limited by the effect of cloud cover and the revisiting cycle (Weng & Yang, 2006). For non-vegetated areas, the satellite sensor measures radiometric temperatures of illuminated surfaces, such as exposed soil and rocky outcrops, but for vegetated surfaces, the sensor captures the temperature close to that identified in the leaf material and in the treetops (Xian & Crane, 2006).

After the transformation of the pixel digital numbers (DN) into radiance, band 10 values were further converted to Kelvin, following the equation (eq. 2):

$$T_{sc} = \frac{K_2}{\ln \ln \left(\frac{K_1}{L_\lambda} + 1 \right)} \quad (2)$$

Tsc refers to temperature without atmospheric correction (Kelvin), K1 is the calibration constant 1 of band 10, K2 is the calibration constant 2 of band 10 and L_λ corresponds to TOA Radiance (Watts) (USGS, 2020). After obtaining the Tsc for each pixel, it was necessary to convert it to Earth's surface temperature (LST), by the following method (eq. 3):

$$T = T_{sc} / \left[1 + \left(\lambda \times \frac{T_{sc}}{c_2} \right) \times \ln(e) \right] \quad (3)$$

Where T refers to the temperature of the Earth's surface (LST - measured in Kelvin), Tsc is the temperature without atmospheric correction (temperature detected in the satellite sensor - in kelvin), λ is the wavelength of the radiance, and refers to the Euler number and c2 refer to the value constant 14388mK, calculated as shown below (eq. 4):

$$c_2 = \frac{h \times c}{s} = 14388 \mu^m K \quad (4)$$

In which h is the Planck constant ($6.62607015 \times 10^{-34}$ J·s), c is the speed of light (2.999×10^8 m/s), and s is the Boltzmann constant (1.38×10^{-23} J/K).

3.4 Vegetation land cover changes

To assess the thermal variation originating from human activity in the studied period, the volume of existing vegetation is used as a comparative parameter. Vegetated areas in cities are presented in many forms, usually characterized in dispersed patches interspersed in the constructed grid (Turrini & Knop, 2015). These spots correspond to parks, squares, gardens and vacant land.

As densification or expansion of urban infrastructure occurs, isolation and conversion of these areas is common, due to the suppression of vegetation. Conversely, if it exhibits dense tree cover, the area can be considered as non-urbanized.

Similarly, as in surface temperature variation analysis, thermal LANDSAT-8 satellite images, of the same period, were used in this situation. To verify the changes in vegetation area in Curitiba, the NDVI (Normalized Vegetation Index Difference) index was used.

NDVI is a dimensionless index derived from the reflectance ratio between red and near infrared, according to the formula (eq. 5):

$$NDVI = (L8\ Band\ 5 - L8\ Band\ 4) \div (L8\ Band\ 5 + L8\ Band\ 4) \quad (5)$$

where NDVI corresponds to the value of -1 to 1, with values closer to 1 refer to dense and healthy vegetation, NIR is the reflectance value in the studied pixel of the near infrared band (band 5 in LANDSAT 8) and R is the value corresponding to the reflectance of the red band (band 4 on LANDSAT 8). As it does not refer to a physical measure, it is in fact dimensionless, but it has an intrinsic relationship with physical characteristics, such as biomass, for example (Carlson & Ripley, 1997)

This equation is derived from the fact that chlorophyll absorbs light of the wavelength corresponding to the red color (approximately 0.630 - 0.680 μm) and the structure of the leaf mesophile reflects the color corresponding to the near infrared (0.845 - 0.885 μm) (Pettorelli et al., 2005), for this reason the NDVI is used as equivalent to the amount of vegetation cover with photosynthetic potential (Xian & Crane, 2006). To assist in visualizing the result, the images were classified and applied to a chromatic scale, between the colors green and red.

NDVI should be used with caution in altered ecosystems, such as cities, due to its high sensitivity to vegetation. In this case, analyzes may erroneously identify degraded vegetation as healthy vegetation, looking only at the outputs of the index. It is essential to observe the results from its application in conjunction with other methodologies (Yengoh et al., 2015)

It is common to apply vegetation indices to understand impermeable surfaces in urban areas, which makes it possible to separate the anthropogenic heat discharge from the natural heat fluxes. Other indices also apply, such as the Normalized Difference Water Index and the Normalized Difference Built-up Index, however, commonly the UHI areas resulting from these methods represent relatively smaller areas (Rahaman et al., 2018)

The data resulting from NDVI are used in this study to assess changes in land use and occupation patterns, and to further calculate land surface emissivity. Since in vegetated areas the documented temperatures are colder and the areas with urban coverage are warmer, when comparing the thermal differences between the years with the patterns of land use and occupation it is possible to identify whether the variation in temperatures is due to changes in territorial coverage, or changes in thermogenic activity patterns in the city.

According to the methodology proposed by Estoque et al. (2017), after calculating the at satellite brightness temperature, it is necessary to perform the conversion for land surface emissivity according to the formula below (eq. 6):

$$\varepsilon = 0.004 P_v + 0.986$$

(6)

In which P_v , is a relation between NDVI, NDVImax and NDVImin to indicate the vegetation proportion as follows (eq. 7):

$$P_v = ((NDVI - NDVI \min) \div (NDVImax + NDVI \min))^2$$

(7)

Through this conversion it is possible to identify the difference in thermal energy emitted and reflected by the various terrestrial surfaces. For interpretation purposes, the absolute value was subtracted from 273.15 to obtain the value in degrees Celsius ($^{\circ}\text{C}$).

3.5 Data analysis

After obtaining the data from the processing of satellite images, validation was performed, comparing them with the data obtained by the local climatological station. Since only two climatological stations are available to check the temperature (in the exact same location), results of a regression analysis would have limited representativeness.

For this, Pearson's correlation coefficient was used to identify if there is a correlation between the temperature averages obtained in the geoprocessed data and the data from the stations. For this, temperature data was obtained from the same hour as the satellite image was taken, and in the resulting raster the temperature was measured from the exact location as the station exists. With this, a pair of data was obtained to use the aforementioned test.

Then, the data obtained in the satellite image processing (as described in the section 3.3) were analysed using the Fisher's exact test to identify whether there are any statistically relevant changes, both for temperature values and vegetation cover values.

The resulting images were classified and applied to a chromatic scale, between the colours blue and red.

The resulting data allows us to observe the spatialization of heat in the city of Curitiba, which occurs due to land use and the heat given off by human activities.

Subsequently, a qualitative analysis of the points at which the greatest thermal variation was identified in this period was performed using data obtained by the Google Maps application, to identify possible changes in anthropogenic thermal emissions in the period of March, and whether there are possible relationships with the period of social detachment derived from combating community transmission of COVID-19.

4 RESULTS AND DISCUSSION

After extracting the data from the satellite scenes, and the subsequent the transformation of radiance into Celsius, it was possible to categorize the minimum, maximum and average temperatures in the month of march from 2018 to 2020 (Table 4). The year of 2020 presents the lowest temperatures in each category.

Table 4 - Landsat 8 Surface Temperature in March 2018, 2019 and 2020

Image	Temperature (°C)		
	Minimum	Maximum	Average
Landsat 8-2018	18,4	31,0	24,9
Landsat 8-2019	15,9	31,8	23,8
Landsat 8-2020	14,9	29,6	23,3

Source: Based on USGS, 2020.

Hourly temperature assessments were extracted from the station A807 to validate the data obtained by the Landsat satellite (Table 5). As explained in section 3

Table 5 - Station Temperature in March 2018, April 2019 and March 2020

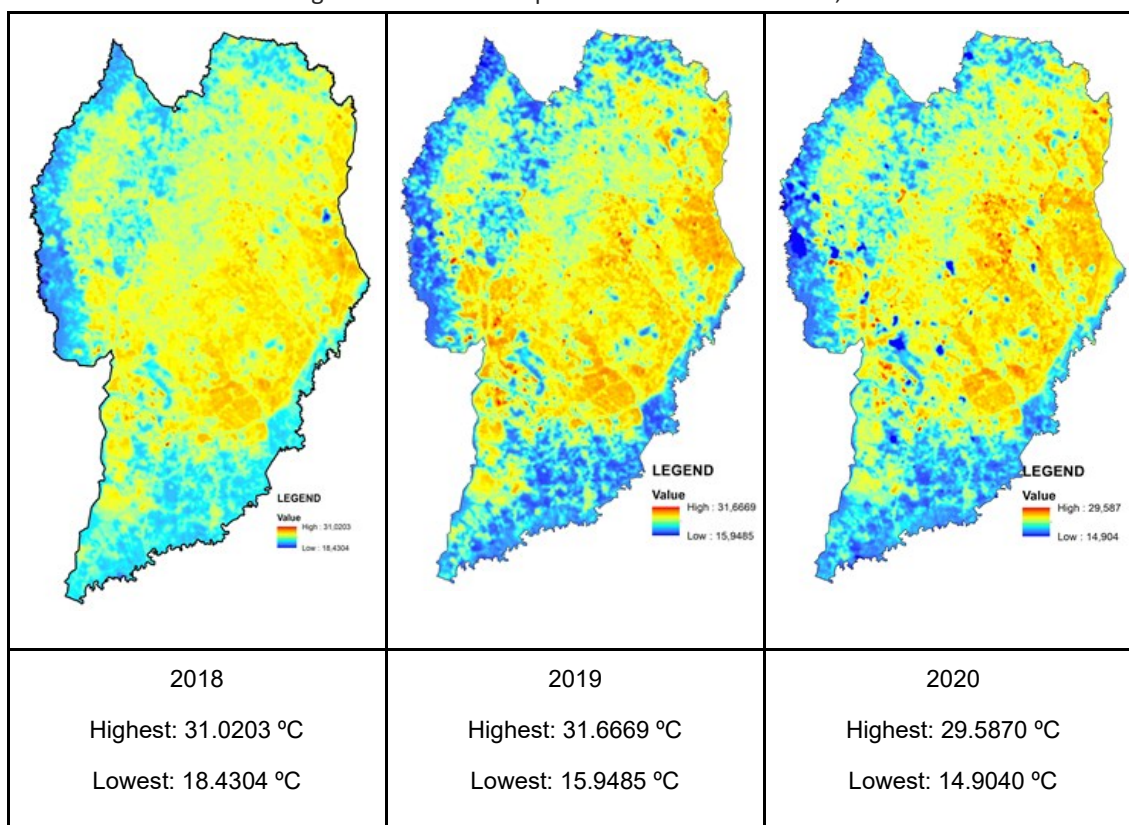
Date	Hour (GMT)	Station temperature (°C)	LS8 temperature - at the spot (°C)
2020-03-19	20:52	26.10	25.90
2019-04-21	20:14	23.00	25.38
2018-03-20	16:10	26.60	25.54

Source: Based on USGS, 2020.

The Pearson correlation coefficient obtained is 0.6133, a moderately strong correlation. This means that the data obtained from station and the information obtained from geoprocessing have a linear correlation. To further validate the temperature maps, more data from stations are needed, which may be a hindrance on studies on geoprocessed UHI in South America or other similar realities. Despite not indicating a strong result robustness, qualitative analyses can be done.

In the surface temperature images for the LANDSAT-8 satellite for the city of Curitiba, it is possible to observe the increase in "blue areas" from one year to another, indicating the decrease in temperature in these areas (Figure 3).

Figure 3 - Surface Temperature of Curitiba in 2018, 2019 and 2020.

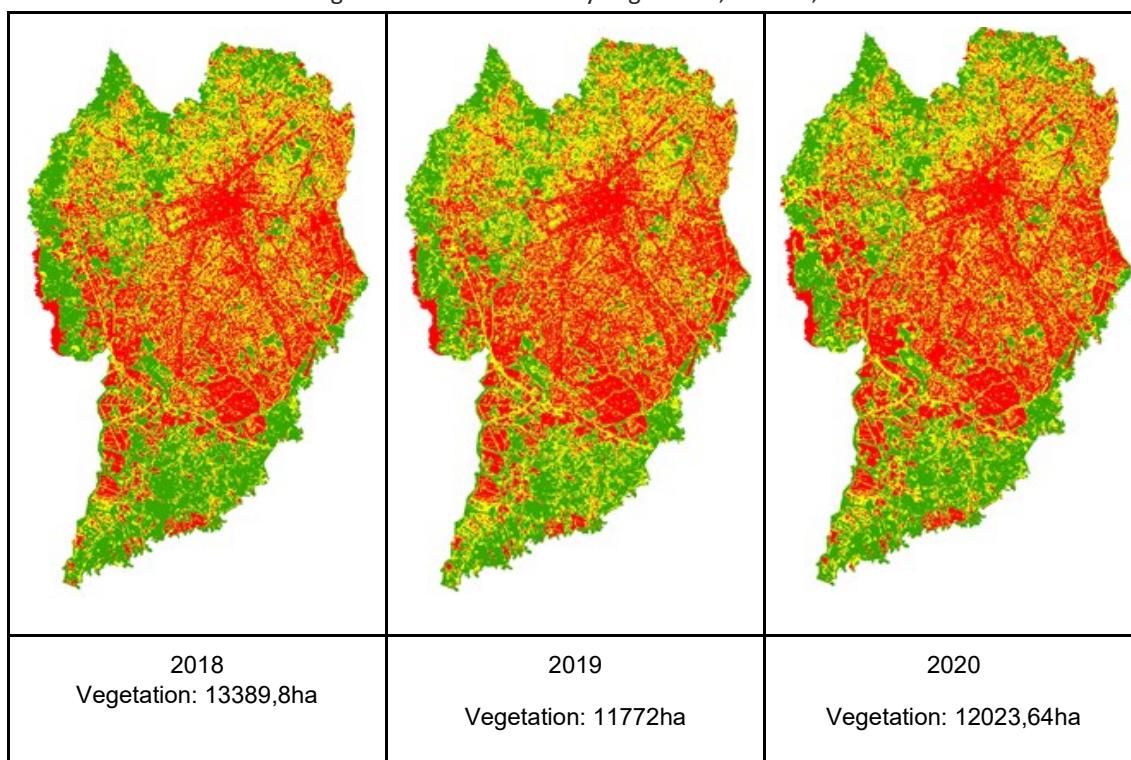


Source: The authors, 2020.

The greatest thermal variation was not found in the densest areas, but in peripheral locations. Conversely, these places have a higher volume of vegetation if compared to the center of Curitiba, but as they present a complex and strategic road network, it may indicate that individual transport has more influence on the temperature variation for Curitiba.

The total vegetation area in the city of Curitiba decreased from 2018 to 2020, from 13389.8ha to 12023.64ha, which constitutes a loss of 1,366.16ha of tree cover (Figure 4) in two years. This increase in transformed land cover has direct implications for the local microclimate, with a high tendency for greater thermal variation throughout the day and the establishment of heat islands in places previously unaffected by the phenomenon.

Figure 4 - Land covered by vegetation, in 2018, 2019 and 2020.



Source: The authors, 2020.

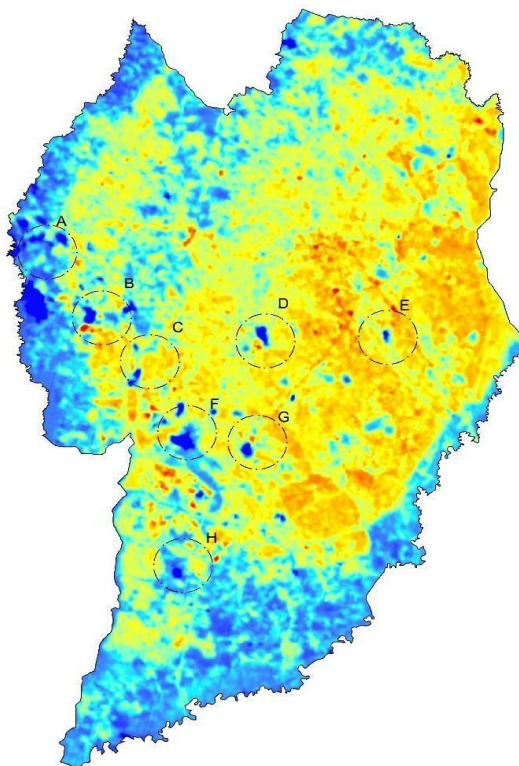
NDVI value oscillation is common in time series, precisely because it is indicative of the photosynthetic activity of the vegetation, which causes it to change in different seasons (Essa et al., 2013). Another issue is related to the seasonality of the climatic events of El Niño and La Niña, which significantly affect rainfall distributions and temperature patterns, consequently modifying photosynthesis.

From the number of pixels obtained in the final raster, it was possible to observe that in the year 2020, at least 60% of the total area has shown temperatures ranging from 23 ° C to 29 ° C. Temperatures below these values added up to a total of 40%.

As the vegetation prevents the wide thermal variation, the extensive forest cover in the city may be related to the low temperature variation between the years studied, except for certain locations. These results were different from the previous year, 2019, in which the average temperatures fluctuated from 15 to 24 ° C in 51% of the whole area. Despite the observed thermal decrease, in 2020 heat spots are scattered across the territory.

In this circumstance, areas of significant size (Figure 5) were detected that showed different results in the year 2020, in thermal terms, compared to previous years. Thus, it was possible to identify places in the city and their peculiarities that led to such a result.









Figure 5 - Areas of Surface Temperature Change in Curitiba.



Source: The authors, 2020.

In figure 6 it is possible to see which characteristics the areas with the greatest positive temperature variation have in common: the building template is low, they are close to green areas (parks, squares, etc.) and are part of important roads (highways or avenues).

Figure 6 - Surface Temperature Change Locations in Curitiba.

			
a) BR 376 X Rod. do Café	b) BR 376 (area with great concentration of industry)	c) Fazendinha	d) Shopping Mall Palladium
			
e) Jardim das Américas	f) Avenida das Indústrias	g) Linha Verde	h) BR 116

Source: The authors, 2020.

One reason for thermal variation within urbanized areas is the spatial occupation parameters. Temperatures are lower in less dense areas, and the heat island effect is scarce.

When observing the selected images, there are areas that are occupied by shopping centers or industry. It is also noteworthy that among the examples presented by shopping malls, (figures 5a and 5d,) these large buildings have open parking lots. In the case of figure 5e, which also has a mall, it has internal parking, but the great influence of this area is given by the large urban roads, which connect Curitiba to the airport.

As for the rest of the examples, they are from the areas that have industry, and similar to the other cases, they bring mostly open parking. Another point of interest in these areas is the high concentration of vegetation in the region.

This variation is consistent with changes in the patterns of travel by motor vehicles in these observed regions (Weng & Yang, 2006). The restrictions imposed by the measures to contain the pandemic caused a reduction in circulation in the road network of the Brazilian city, which corresponds to the contraction of heat emanation by motor vehicles, which may also suggest a contraction in the emission of pollutants by these modes. From the locations shown in Figure 2, the temperatures of these areas were also identified (Table 6).

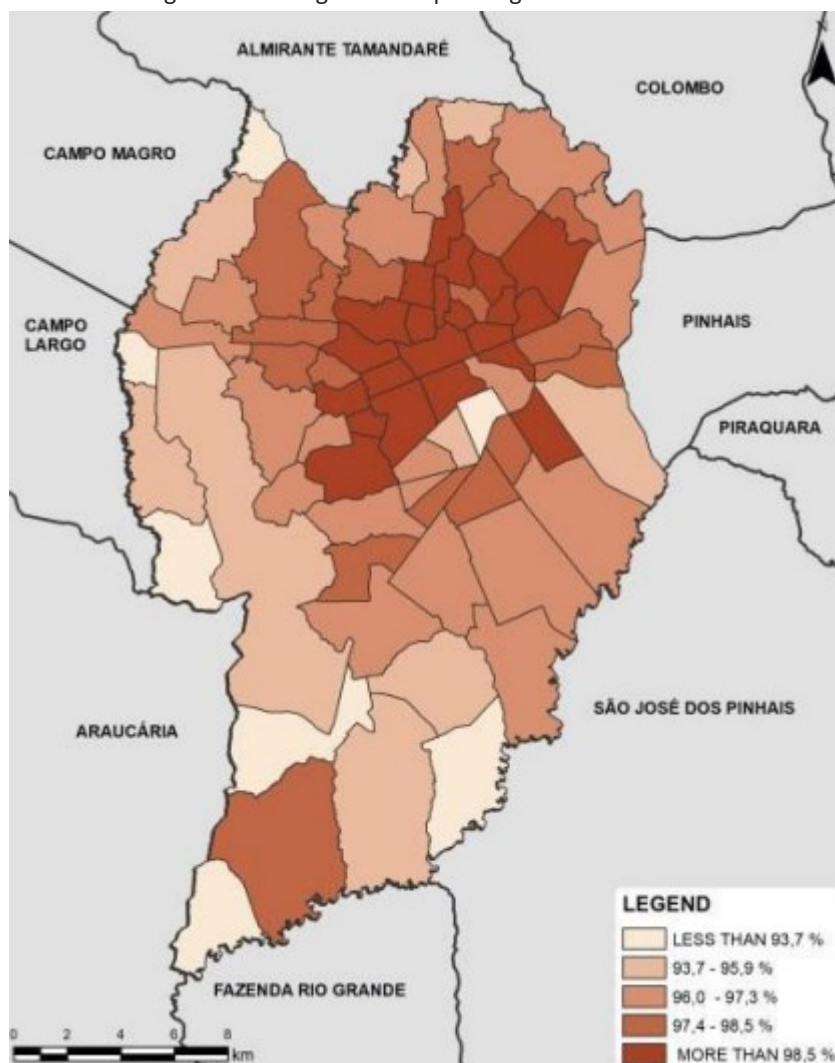
Table 6 - Surface temperature at the main variation points

Point	Temperature (°C)			
	Mínimum (2020)	Maximum (2019)	Average	Variation
A	18,3	25,5	21,9	7,2
B	16,2	27,8	22	11,6
C	18,9	29,1	24	10,2
D	16,7	28,6	22,65	11,9
E	18,2	29,6	23,9	11,4
F	16,1	29,4	22,75	13,3
G	17,3	25,7	21,5	8,4
H	17,6	20,2	18,9	2,6

Source: The authors, 2020.

When referring to information related to the neighborhoods (Figure 7) where the main temperature changes in the city are located, it is seen that these are made up of places with the lowest average wage.

Figure 7 - Average income per neighborhood in Curitiba.



Source: Pellizzaro et al, 2018.

The regions that most had temperature variation and by looking at figure 6, it is possible to identify that they are the neighborhoods with the lowest average income in Curitiba. Unlike central areas, which tend to have the tallest buildings in the city, in these regions, however, they are more distant and smaller.

Central places, and other types of urban nodes, are a focal point of capital and mobility flows, therefore little affected by the turnarounds of the social isolation initiative.

Beyond the vicissitudes of the pandemic by itself, the mitigation initiatives such as social isolation might prove to be a hurdle to low income and vulnerable citizens, due to constrictions on the industry and services sector, opposed to other types of economic activities developed in the richest localities of the city.

5 CONCLUSIONS

The COVID-19 pandemic has generated numerous changes in society, which has brought many territorial changes at various spatial scales. One of them is the impact on the thermal balance caused by the reduction of social activities. This article observed this phenomenon through the analysis of satellite images and geoprocessing, resulting in specialized data on heat emissions in the city. The conclusions that emerge from this analysis are:

- With the decrease in social and economic activities, due to COVID-19, there was a decrease in surface temperature in certain locations in the city of Curitiba.
- Places with a large area of exposed surface, such as shopping malls and industries, had the greatest temperature variation.
- Highways and major roads (wide roads) in the city (which have a large flow of vehicles) were also areas that decreased the temperature, thus showing the impact of vehicles in relation to heat emission.
- The analytical method proved to be adequate, since there is a linear correlation between the data provided by the raster and the data from local stations, despite limitations for its validation.

ACKNOWLEDGEMENTS

To the Coordination for the Improvement of Higher Education Personnel (Coordenação de Aperfeiçoamento de Pessoal de Nível Superior - CAPES), for the scholarship funding of the Support Program for the Post-Graduation of Community Institutions of Higher Education (PROSUC), and to the Araucária Foundation for the Support of Scientific and Technological Development of the State of Paraná (Fundação Araucária de Apoio ao Desenvolvimento Científico e Tecnológico do Estado do Paraná - FAADCT-PR), for the scholarship financing of the Social Demand Program (DS-CAPES).

To the National Council for Scientific and Technological Development (Conselho Nacional de Desenvolvimento Científico e Tecnológico - CNPq).

Landsat-8 image courtesy of the U.S. Geological Survey.

Consequências da covid-19: variação térmica urbana e repercussão social

RESUMO

A variação térmica é um fenômeno urbano comum, de pequenas a grandes cidades, tanto por sua origem antrópica quanto por causas naturais. Por influência da COVID 19, houve redução das atividades sociais, principalmente econômicas, que impactou tanto a produção industrial quanto a diminuição da circulação de veículos. Essas mudanças de hábitos afetam a dinâmica térmica urbana. Assim, o objetivo do estudo é identificar se a redução das atividades socioeconômicas afetou os padrões de variação térmica em Curitiba, Brasil. Para esta análise, foram utilizadas imagens Landsat 8 dos anos 2018, 2019 e 2020 para verificar a variação da temperatura na região, e o índice NDVI foi aplicado para verificar a variação da área permeável na capital. Assim, foi possível observar que a temperatura média total da superfície de Curitiba diminuiu 1,6 ° C. Verificou-se também que em algumas áreas a redução foi maior do que em outras, e a variação entre a temperatura mínima e máxima foi de 13,3 ° C. Vale ressaltar que devido à redução das áreas verdes na região, era esperado um aumento da temperatura. As áreas com maior variação de temperatura em graus foram aquelas com grandes vias em Curitiba, locais cuja população ganha salários baixos em comparação com os bairros mais centrais da cidade. Embora o vírus gere grande preocupação com a saúde da população, pode-se observar uma queda significativa da temperatura, causada principalmente pela circulação de veículos.

PALAVRAS-CHAVE: Ilha de Calor Urbano, Saúde Ambiental, Landsat 8

REFERENCES

- Anderson, R., Heesterbeek, H., Klinkenberg, D., & Hollingsworth, T. (2020). How will country-based mitigation measures influence the course of the COVID-19 epidemic?. *The Lancet*, 395(10228), 931-934. [https://doi.org/10.1016/s0140-6736\(20\)30567-5](https://doi.org/10.1016/s0140-6736(20)30567-5)
- Andersson, E. (2018). Functional landscapes in cities: a systems approach. *Landscape and ecological engineering*, 14(2), 193-199. <https://doi.org/10.1007/s11355-017-0346-6>
- Araújo, M. R. M. D., Oliveira, J. M. D., Jesus, M. S. D., Sá, N. R. D., Santos, P. A. C. D., & Lima, T. C. (2011). Collective public transportation: discussing accessibility, mobility and quality of life. *Psicologia & Sociedade*, 23(3), 574-582. <https://doi.org/10.1590/S0102-71822011000300015>
- Barbosa, R. V. R. (2009). Estudo do campo térmico urbano de São Carlos (SP): análise da intensidade da ilha de calor urbano em episódio climático de verão (Doctoral dissertation, Universidade de São Paulo).
- Bedford, J., Enria, D., Giesecke, J., Heymann, D. L., Ihekweazu, C., Kobinger, G., ... & Ungchusak, K. (2020). COVID-19: towards controlling of a pandemic. *The Lancet*, 395(10229), 1015-1018. [https://doi.org/10.1016/S0140-6736\(20\)30673-5](https://doi.org/10.1016/S0140-6736(20)30673-5)
- Boareto, R. (2008). A política de mobilidade urbana e a construção de cidades sustentáveis. *Revista dos Transportes Públicos-ANTP-Ano*, 30, 31-2008.
- Carlson, T. N., & Ripley, D. A. (1997). On the relation between NDVI, fractional vegetation cover, and leaf area index. *Remote Sensing of Environment*, 62(3), 241-252. [https://doi.org/10.1016/S0034-4257\(97\)00104-1](https://doi.org/10.1016/S0034-4257(97)00104-1)
- Curitiba (PR) | Cidades e Estados | IBGE. ibge.gov.br. (2020). Retrieved 15 April 2020, from <https://www.ibge.gov.br/cidades-e-estados/pr/curitiba.html>.
- Ding, H., & Shi, W. (2013). Land-use/land-cover change and its influence on surface temperature: a case study in Beijing City. *International Journal of Remote Sensing*, 34(15), 5503-5517. <https://doi.org/10.1080/01431161.2013.792966>
- El Niño & La Niña (El Niño-Southern Oscillation) | NOAA Climate.gov. Climate.gov. (2020). Retrieved 15 April 2020, from <https://www.climate.gov/enso>.

Essa, W., van der Kwast, J., Verbeiren, B., & Batelaan, O. (2013). Downscaling of thermal images over urban areas using the land surface temperature–impervious percentage relationship. *International Journal of Applied Earth Observation and Geoinformation*, 23, 95-108. <http://dx.doi.org/10.1016/j.jag.2012.12.007>

Estoque, R. C., Murayama, Y., & Myint, S. W. (2017). Effects of landscape composition and pattern on land surface temperature: An urban heat island study in the megacities of Southeast Asia. *Science of the Total Environment*, 577, 349–359. <https://doi.org/10.1016/j.scitotenv.2016.10.195>

Ferreira, F., & Andrade, W. (2021). Urban Climate Assessment of Urban Heat Islands in Brazil based on MODIS remote sensing data. *Urban Climate*, 35(November 2020). <https://doi.org/10.1016/j.uclim.2020.100726>

Forster, P. M., Forster, H. I., Evans, M. J., Gidden, M. J., Jones, C. D., Keller, C. A., Lamboll, R. D., Quéré, C. Le, Rogelj, J., Rosen, D., Schleussner, C. F., Richardson, T. B., Smith, C. J., & Turnock, S. T. (2020). Current and future global climate impacts resulting from COVID-19. *Nature Climate Change*, 10(10), 913–919. <https://doi.org/10.1038/s41558-020-0883-0>

Golden, J. S. (2004). The built environment induced urban heat island effect in rapidly urbanizing arid regions—a sustainable urban engineering complexity. *Environmental Sciences*, 1(4), 321-349. <https://doi.org/10.1080/15693430412331291698>

Google Maps. Google Maps. (2020). Retrieved 26 May 2020, from <https://www.google.com/maps>.

Haddad, L., & Aouachria, Z. (2015). Impact of the transport on the urban heat island. *International Journal of Environmental and Ecological Engineering*, 9(8), 968-973. [https://doi.org/10.7708/ijtte.2015.5\(3\).03](https://doi.org/10.7708/ijtte.2015.5(3).03)

Instituto Nacional de Meteorologia - INMET | Normais Climatológicas. Instituto Nacional de Meteorologia. (2020). Retrieved 4 October 2020, from <http://portal.inmet.gov.br/servicos/normais-climatol%C3%B3gicas>.

Instituto Nacional de Meteorologia - INMET (2021). Banco de dados meteorológicos para ensino e pesquisa. BDMEP. Retrieved 17 March 2021, from <https://bdmep.inmet.gov.br/>

Instituto de Pesquisa e Planejamento Urbano de Curitiba - IPPUC. (2013). Consolidação de dados de Oferta, Demanda, Sistema Viário e Zoneamento: Relatório 5 – Pesquisa Origem – Destino Domiciliar. Curitiba.

Instituto de Pesquisa e Planejamento Urbano de Curitiba – IPPUC. (2020). Dados Geográficos. Retrieved 3 April 2020, from <https://ippuc.org.br/geodownloads/geo.htm>

Instituto de Terras, Cartografia e Geologia do Paraná - ITCG. [Itcg.pr.gov.br](http://www.itcg.pr.gov.br). (2020). Retrieved 21 April 2020, from <http://www.itcg.pr.gov.br/modules/faq/category.php?categoryid=9#>.

Keil, R., & Ali, H. (2007). Governing the sick city: urban governance in the age of emerging infectious disease. *Antipode*, 39(5), 846-873. <https://doi.org/10.1111/j.1467-8330.2007.00555.x>

Kolbe, K. (2019). Mitigating urban heat island effect and carbon dioxide emissions through different mobility concepts: Comparison of conventional vehicles with electric vehicles, hydrogen vehicles and public transportation. *Transport Policy*, 80, 1-11. <https://doi.org/10.1016/j.tranpol.2019.05.007>.

Kowarik, I. (2011). Novel urban ecosystems, biodiversity, and conservation. *Environmental pollution*, 159(8-9), 1974-1983. <https://doi.org/10.1016/j.envpol.2011.02.022>

Krüger, E. L. (2015). Landscape and Urban Planning Urban heat island and indoor comfort effects in social housing dwellings. *Landscape and Urban Planning*, 134, 147–156. <https://doi.org/10.1016/j.landurbplan.2014.10.017>

Lapola, D. M., Braga, D. R., Giulio, G. M. Di, Torres, R. R., & Vasconcellos, M. P. (2019). Heat stress vulnerability and risk at the (super) local scale in six Brazilian capitals. *Climatic Change*, 154, 477–492. <https://doi.org/https://doi.org/10.1007/s10584-019-02459-w>

Lunardon, K.A.F., 2017. Aspectos do clima urbano de Curitiba/PR: Uma abordagem do campo térmico e sua influência sobre a ocorrência da dengue. *Os Desafios da Geografia Física na Fronteira do Conhecimento* 1, 2572–2576.

Neves, G., Gallardo, N., Felício, R., Macedo, S., & Vecchia, F. (2018). Variação da temperatura de superfície em diferentes usos do solo na cidade de São Carlos-SP. *GOT, Revista de Geografia e Ordenamento do Território*, (13), 315-336. <http://dx.doi.org/10.17127/got/2018.13.014>

Nichol, J., & Wong, M. S. (2005). Modeling urban environmental quality in a tropical city. *Landscape and urban planning*, 73(1), 49-58. <https://doi.org/10.1016/j.landurbplan.2004.08.004>

Palme, M., Lobato, A., & Carrasco, C. (2016). Quantitative Analysis of Factors Contributing to Urban Heat Island Effect in Cities of Latin-American Pacific Coast. *Procedia Engineering*, 169, 199–206.
<https://doi.org/10.1016/j.proeng.2016.10.024>

Pettorelli, N., Vik, J. O., Mysterud, A., Gaillard, J. M., Tucker, C. J., & Stenseth, N. C. (2005). Using the satellite-derived NDVI to assess ecological responses to environmental change. *Trends in ecology & evolution*, 20(9), 503-510.
<https://doi.org/10.1016/j.tree.2005.05.011>

Pellizzaro, P. C., Hardt, L. P. A., Hardt, C., Tanaka, M. (2018). Social and environmental vulnerability of the urban dynamics of Curitiba, Paraná, Brazil. *Australian Journal of Basic and Applied Sciences*. 12(7), 165-171.
<https://www.doi.org/10.22587/ajbas.2018.12.7.24>

Rahaman, K. R., Ahmed, M. R., & Hassan, Q. K. (2018). Using satellite-borne remote sensing data in generating local warming maps with enhanced resolution. *ISPRS International Journal of Geo-Information*, 7(10).
<https://doi.org/10.3390/ijgi7100398>

Rahaman, K. R., Hassan, Q. K., & Chowdhury, E. H. (2017). Quantification of local warming trend: A remote sensing-based approach. *PLoS ONE*, 12(1), 1–18.
<https://doi.org/10.1371/journal.pone.0169423>

Roy, D. P., Kovalsky, V., Zhang, H. K., Vermote, E. F., Yan, L., Kumar, S. S., & Egorov, A. (2016). Characterization of Landsat-7 to Landsat-8 reflective wavelength and normalized difference vegetation index continuity. *Remote Sensing of Environment*, 185, 57–70. <https://doi.org/10.1016/j.rse.2015.12.024>

Sánchez-Reyes, U. J., Niño-Maldonado, S., Barrientos-Lozano, L., & Treviño-Carreón, J. (2017). Assessment of land use-cover changes and successional stages of vegetation in the natural protected area Altas Cumbres, Northeastern Mexico, using Landsat satellite imagery. *Remote Sensing*, 9(7), 712.
<https://doi.org/10.3390/rs9070712>.

Turrini, T., & Knop, E. (2015). A landscape ecology approach identifies important drivers of urban biodiversity. *Global change biology*, 21(4), 1652-1667.
<https://doi.org/10.1111/gcb.12825>

USGS – Science for a Changing World. EarthExplorer. Retrieved 15 April 2020 From <https://earthexplorer.usgs.gov/>

Wang, P., Chen, K., Zhu, S., Wang, P., & Zhang, H. (2020). Severe air pollution events not avoided by reduced anthropogenic activities during COVID-19 outbreak. *Resources, Conservation and Recycling*, 158, 104814. <https://doi.org/10.1016/j.resconrec.2020.104814>

Weng, Q., & Yang, S. (2006). Urban air pollution patterns, land use, and thermal landscape: an examination of the linkage using GIS. *Environmental monitoring and assessment*, 117(1-3), 463-489. <https://doi.org/10.1007/s10661-006-0888-9>

WHO Coronavirus Disease (COVID-19) Dashboard. Covid19.who.int. (2020). Retrieved 10 April 2020, from <https://covid19.who.int/>.

Xian, G., & Crane, M. (2006). An analysis of urban thermal characteristics and associated land cover in Tampa Bay and Las Vegas using Landsat satellite data. *Remote Sensing of environment*, 104(2), 147-156. <https://doi.org/10.1016/j.rse.2005.09.023>

Yamak, B., Yağci, Z., Bilgilioglu, B. B., & Çömert, R. (2021) Investigation of the effect of urbanization on land surface temperature example of Bursa. *International Journal of Engineering and Geosciences*, 6(1), 1-8. <https://doi.org/10.26833/ijeg.658377>

Yin, C., Yuan, M., Lu, Y., Huang, Y., & Liu, Y. (2018). Effects of urban form on the urban heat island effect based on spatial regression model. *Science of the Total Environment*, 634, 696-704. <https://doi.org/10.1016/j.scitotenv.2018.03.350>

Zhang, N., Huang, H., Su, B., Ma, X., & Li, Y. (2018). A human behavior integrated hierarchical model of airborne disease transmission in a large city. *Building and Environment*, 127(November 2017), 211–220. <https://doi.org/10.1016/j.buildenv.2017.11.011>

Recebido: 07 mai. 2022.

Aprovado: 23 mai. 2022.

DOI: 10.3895/rbpd.v11n3.esp.14382

Como citar: AZZULIN, M. B.; JEDYN, A.; CENTURION, N.; FERNANDES, C. Consequences of covid-19: urban thermal variation and social repercussion. *R. bras. Planej. Desenv.* Curitiba, v. 11, n. 03, p. 844-869, set./dez. 2022. Disponível em: <<https://periodicos.utfpr.edu.br/rbpd>>. Acesso em: XXX.

Correspondência:

Mayara Bormann Azzulin

Av. Sete de Setembro, 3165 - Rebouças, Curitiba - PR

Direito autoral: Este artigo está licenciado sob os termos da Licença Creative Commons-Atribuição 4.0 Internacional.

